Annals of Mathematical Sciences and Applications
Volume 5, Number 1, 75–100, 2020

A direct-forcing immersed boundary projection method for simulating the dynamics of freely falling solid bodies in an incompressible viscous fluid*

Po-Wen Hsieh, Suh-Yuh Yang†, and Cheng-Shu You†

In this paper, we develop a new direct-forcing immersed boundary approach combined with the Choi-Moin projection scheme for simulating the dynamics of freely falling solid bodies in an incompressible viscous fluid. At first, the solid object region is regarded as made of fluid and we then introduce a virtual force distributed only on that region that enforces it to behave like a real solid body with the solid velocity. The time integration of the momentum equation is performed by using a third-order Runge-Kutta formula for the convection and a second-order Crank-Nicolson formula for the diffusion. Moreover, second-order centered differences over a staggered Cartesian grid are employed for all the spatial discretizations in the projection scheme. We also integrate a collision model into the method for circular particles to mimic the repulsion force arising from body-body or body-wall collisions in the fluid-solid interaction process. The most advantageous feature of the proposed method is that it is conceptually simple and rather easy to implement without involving any discrete Dirac delta functions or post interpolations for accuracy like most immersed boundary methods in the literature. Several numerical experiments are carried out to illustrate the effectiveness of the newly proposed method.

AMS 2000 subject classifications: Primary 65M06; secondary 76M20.

Keywords and phrases: Incompressible Navier-Stokes equations, fluid-solid interaction, free falling body, sedimentation, immersed boundary method, direct-forcing method, projection scheme.

*This work was supported by the Ministry of Science and Technology of Taiwan under grants MOST 106-2115-M-005-005-MY2 (Po-Wen Hsieh), MOST 106-2115-M-008-014-MY2 (Suh-Yuh Yang), and MOST 107-2115-M-035-007-MY2 (Cheng-Shu You). The research of Suh-Yuh Yang was also partially supported by the National Center for Theoretical Sciences, Taiwan.

†Corresponding authors.

1. Introduction

The main purpose of this paper is to develop a new direct-forcing immersed boundary approach combined with the Choi-Moin projection scheme for simulating the dynamics of freely falling solid bodies in an incompressible viscous fluid. It is well known that the interaction between moving solid object and fluid may display complicated and even unpredictable behavior. A typical example is the freely falling plate in an incompressible viscous fluid that can exhibit rich dynamical behavior such as fluttering, looping, and tumbling motions, see, e.g., [1, 2, 3, 12, 14, 19, 20, 26, 29, 30, 32, 36, 37] and many references cited therein. However, due to the geometrical complexity encountered in the moving boundary problems, it is still challenging and computationally expensive to simulate such kind of two-way fluid-solid interaction (FSI) problems by using the conventional body-fitted approach.

A powerful Cartesian grid based non-boundary conforming method for simulating the dynamics of FSI problems with moving boundaries is the so-called immersed boundary (IB) method which was first developed in the 1970s by Peskin [38, 39]. In the IB method, the immersed structure exerts a force on the fluid, and the interaction between structure and fluid can be represented by a contribution to the forcing term in the fluid momentum equation. Instead of generating a boundary-fitted grid to the immersed boundary at each time step, the spatial discretization of the IB method is implemented over Cartesian grids for the entire domain and the immersed boundary is discretized by a set of Lagrangian marker points that are not constrained to lie on the grids. Broadly speaking, the existing IB methods can be divided into the feedback-forcing and direct-forcing approaches, according to how the momentum-forcing term associated with the method is generated [31]. For the past two decades, due to its conceptual simplicity and computational efficiency, the direct-forcing approach has been attracted a lot of attention, see e.g., [8, 11, 15, 23, 26, 27, 28, 33, 41, 42, 43, 44, 45] and many references cited herein.

In the works [21, 22] of Kajishima *et al.*, see also [34], a simple direct-forcing IB approach combined with the first-order in time Chorin projection scheme [6, 7] has been successfully developed. In contrast to most direct-forcing IB methods in the literature, the momentum forcing introduced in that method, called the virtual force [34] here, is not just distributed on the immersed solid boundary, but is actually distributed on the whole solid body region. Moreover, the solid object region is regarded as made of fluid, but the virtual force enforces the region to behave like a real solid body with the solid velocity. In other words, this virtual force plays the role of

momentum forcing term to accommodate the interaction between solid and fluid. The major advantage of this method is its simplicity in implementation when combining with the projection schemes. Although this direct-forcing IB method can produce reasonable results for simulating many FSI applications, we have pointed out in [18] that it is not always convergent if the method is combined with an arbitrarily chosen projection scheme, unless the time step is chosen sufficiently small. The reason for this failure is the inconsistency between velocity and pressure at the end of each time step with velocity being changed but not pressure in the immersed solid region. This particularly causes a problem in calculating the intermediate velocity of the next time step when employing pressure from the previous time step. We therefore provided a two-stage prediction-correction approach in [18] to alleviate the inconsistency arising in the method [21, 22, 34].

It was also pointed out in [18] that in the direct-forcing IB method [21, 22, 34], the divergence-free condition may be destroyed in cut cells in a Cartesian grid of the fluid domain at which the solid-fluid interface is located. However, from the numerical results of the problem of flow over a cylinder reported in [18], we can find that the divergence-free condition of the method is generally satisfied except only at the leading edge of cylinder. To observe more carefully, we can also find that these non-zero divergence spots appear as pairs of mass sink and source of equal magnitude (doublet), which upholds global mass conservation of the method.

In this paper, we will continue the study of this simple direct-forcing IB projection approach for numerical simulations of the FSI problems with freely falling solid bodies in an incompressible viscous fluid. We will combine the direct-forcing IB approach with the Choi-Moin second-order in time projection scheme [5] instead of the Chorin first-order scheme. We remark that the Choi-Moin projection scheme is particularly suitable for this direct-forcing IB approach which has been discussed in [18]. The key idea of this newly proposed method is still based on introducing a virtual fluid force. We first treat the solid object region as made of fluid and then introduce a virtual force distributed only on that region to make the region behaving like a real solid body with the solid velocity. Certainly, the role of the virtual force plays is to accommodate the interaction between solid and fluid such that the unsteady velocity boundary condition at the immersed solid boundary can be appropriately satisfied.

In the present method, the time integration of the momentum equation is performed by using a third-order Runge-Kutta formula for the convection term and a second-order Crank-Nicolson formula for the diffusion term [16, 17, 25]. Moreover, second-order centered differences over a staggered

Cartesian grid are employed for all the spatial discretizations in the projection scheme. We also integrate a collision model into the method for circular particles to mimic the repulsion force arising from body-body or body-wall collisions in the fluid-solid interaction process, if necessary. The most advantageous feature of this method is that it is conceptually simple and rather easy to implement, without involving any discrete Dirac delta functions or any post interpolations for accuracy like most IB methods in the literature. We will perform several numerical experiments to illustrate the effectiveness of the proposed method. To validate the method, we first consider the flow past a swimming fish-like solid body with a given varying solid shape and a prescribed solid velocity. We then study the falling of a single circular solid ball and two circular solid balls in a rectangular tank filled with an incompressible Newtonian viscous fluid, and the sedimentation of a cloud of circular particles in a non-rectangular fluid domain. We can find that the obtained results are in very good agreement with the previous works in the literature.

The remainder of this paper is organized as follows. In Section 2, we introduce the basic idea of the direct-forcing approach for solving FSI problems and derive the governing equations of motion of a freely falling solid body. In Section 3, a simple collision model is presented. In Section 4, we propose the direct-forcing IB projection method with all the details. Several numerical experiments are carried out in Section 5. Finally, a summary and conclusions are given in Section 6.

2. The governing equations of FSI problems

In this section, we consider for simplicity a two-dimensional bounded fluid domain $\Omega \subset \mathbb{R}^2$ that encloses a single freely falling solid body positioned at $\overline{\Omega}_s(t)$, where the solid velocity $\boldsymbol{u}_s(t, \boldsymbol{x})$ obeys the equations of motion that will be derived later. The cases of three-dimensional fluid domain and multiple freely falling solid bodies can be treated in a similar way.

In the direct-forcing IB approach, we first regard the solid object region as made of fluid and then introduce a virtual force $\boldsymbol{F}$ distributed only on the region $\overline{\Omega}_s$ that enforces the region to behave like a real solid body with the solid velocity. Actually, the virtual force will be incorporated into the equations of motion of the immersed solid object and also appended to the momentum equations of the incompressible Navier-Stokes equations to accommodate the interaction between the solid and fluid such that the velocity boundary condition at the immersed boundary is satisfied. Later on, we will

specify such virtual force in its discrete version in the projection computations. Let $\boldsymbol{u}$ be the velocity field, p the pressure (divided by a constant fluid density ρ_f), ν the kinematic viscosity, and $\boldsymbol{f}$ the density of body force. In general, $\boldsymbol{f}$ will be set to zero for two-dimensional fluid domains. At this moment, the governing equations of the dynamics of the freely falling solid in an incompressible viscous fluid can be posed as follows:

$$
\begin{aligned}
\frac{\partial \boldsymbol{u}}{\partial t} - \nu \nabla^2 \boldsymbol{u} + (\boldsymbol{u} \cdot \nabla)\boldsymbol{u} + \nabla p &= \boldsymbol{f} + \boldsymbol{F}, \quad t \in (0,T),\ \boldsymbol{x} \in \Omega, \\
\nabla \cdot \boldsymbol{u} &= 0, \quad t \in (0,T),\ \boldsymbol{x} \in \Omega, \\
\boldsymbol{u} &= \boldsymbol{u}_s \quad t \in (0,T),\ \boldsymbol{x} \in \overline{\Omega}_s, \\
\boldsymbol{u} &= \boldsymbol{u}_b, \quad t \in (0,T),\ \boldsymbol{x} \in \partial\Omega, \\
\boldsymbol{u} &= \boldsymbol{u}_0, \quad t = 0,\ \boldsymbol{x} \in \overline{\Omega},
\end{aligned}
\tag{2.1}
$$

where $\boldsymbol{F}$ is the virtual force to make $\boldsymbol{u} = \boldsymbol{u}_s$ on $\overline{\Omega}_s$ for $t \in (0,T)$ and $\boldsymbol{u}_s$ is the velocity of the immersed solid body which obeys the equations of motion as described below.

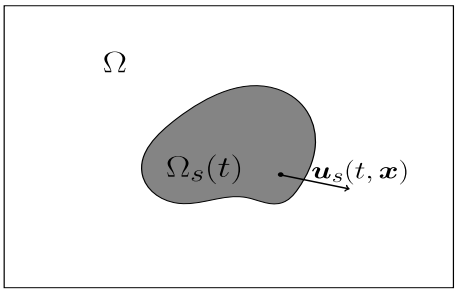

Figure 2.1: A schematic diagram of a moving solid body $\overline{\Omega}_s(t)$.

To derive the equations of motion of the solid body immersed in an incompressible viscous fluid, we mainly follow the ideas of [35, 45]. In Newton's mechanics, the dynamics of freely falling solid in an incompressible viscous fluid is determined by the gravitational force, the buoyancy force and the hydrodynamic force due to the interaction between solid and fluid. Consider a solid object of constant density ρ_s positioned at $\overline{\Omega}_s$, whose centroid is located at $\boldsymbol{X}_c$ and moves at translational velocity $\boldsymbol{u}_c$ and angular velocity ω. Then the velocity of the solid object is given by

$$
\boldsymbol{u}_s(t,\boldsymbol{x}) = \boldsymbol{u}_c(t) + \omega(t) \times \boldsymbol{r}(t,\boldsymbol{x}),
\tag{2.2}
$$

for all $\boldsymbol{x} \in \overline{\Omega}_s(t)$, where $\boldsymbol{r} = (r_1, r_2) := \boldsymbol{x} - \boldsymbol{X}_c$ and

$$\omega(t) \times \boldsymbol{r}(t, \boldsymbol{x}) := \big(-\omega(t) r_2(t, \boldsymbol{x}), \omega(t) r_1(t, \boldsymbol{x})\big)^\top.$$

Notice that

$$\frac{d\boldsymbol{X}_c}{dt} = \boldsymbol{u}_c \quad \text{and} \quad \frac{d\theta}{dt} = \omega, \tag{2.3}$$

where θ is the rotational angle in counter-clockwise.

First, we imagine that the solid object region is made of fluid and there is a virtual force $\boldsymbol{F}$ distributed on the region $\overline{\Omega}_s$. Taking the control volume Ω_s for the momentum equation, from Newton's second law, we have

$$\frac{d\boldsymbol{u}_c}{dt} \int_{\Omega_s} \rho_f \, dV = \int_{\partial\Omega_s} \boldsymbol{\sigma} \cdot \boldsymbol{n} \, dS + \int_{\Omega_s} \rho_f \boldsymbol{F} \, dV + \int_{\Omega_s} \rho_f \boldsymbol{g} \, dV, \tag{2.4}$$

$$I_f \frac{d\omega}{dt} = \int_{\partial\Omega_s} \boldsymbol{r} \times (\boldsymbol{\sigma} \cdot \boldsymbol{n}) \, dS + \int_{\Omega_s} \rho_f \boldsymbol{r} \times \boldsymbol{F} \, dV, \tag{2.5}$$

where $\boldsymbol{\sigma} = -p\boldsymbol{I} + 2\mu_f \boldsymbol{\varepsilon}(\boldsymbol{u})$ is the stress tensor of the fluid, $\boldsymbol{\varepsilon}(\boldsymbol{u})$ is the rate of strain tensor, μ_f is the dynamic viscosity, $\boldsymbol{n}$ is the outward unit normal vector to $\partial\Omega_s$, ρ_f is the density of fluid, $\boldsymbol{g}$ is the gravity, $I_f = \int_{\Omega_s} \rho_f |\boldsymbol{r}|^2 \, dV$ is the rotational inertia for the fluid.

On the other hand, the motion of solid object can also be described by the translational and angular momentum of the solid body and thus we have

$$\frac{d\boldsymbol{u}_c}{dt} \int_{\Omega_s} \rho_s \, dV = \int_{\partial\Omega_s} \boldsymbol{\sigma} \cdot \boldsymbol{n} \, dS + \int_{\Omega_s} \rho_s \boldsymbol{g} \, dV, \tag{2.6}$$

$$I_s \frac{d\omega}{dt} = \int_{\partial\Omega_s} \boldsymbol{r} \times (\boldsymbol{\sigma} \cdot \boldsymbol{n}) \, dS, \tag{2.7}$$

where $I_s = \int_{\Omega_s} \rho_s |\boldsymbol{r}|^2 \, dV$ is the rotational inertia for the solid object.

In fact, the virtual force $\boldsymbol{F}$ makes (2.4)-(2.5) equivalent to (2.6)-(2.7). Now, we have the following equations of motion:

$$\frac{d\boldsymbol{u}_c}{dt} \int_{\Omega_s} (\rho_s - \rho_f) \, dV = \int_{\Omega_s} (\rho_s - \rho_f) \boldsymbol{g} \, dV - \int_{\Omega_s} \rho_f \boldsymbol{F} \, dV, \tag{2.8}$$

$$(I_s - I_f) \frac{d\omega}{dt} = -\int_{\Omega_s} \rho_f \boldsymbol{r} \times \boldsymbol{F} \, dV. \tag{2.9}$$

The first and second terms in the right hand side of (2.8) represent the difference of gravity and buoyant force and the drag force, respectively. The

equation (2.8) can be further expressed as

$$(M_s - M_f)\frac{d\boldsymbol{u}_c}{dt} = (M_s - M_f)\boldsymbol{g} - \int_{\Omega_s} \rho_f \boldsymbol{F}\, dV, \tag{2.10}$$

where the solid mass M_s and the fluid mass M_f of the region Ω_s are respectively defined by

$$M_s := \int_{\Omega_s} \rho_s\, dV = \int_{\Omega} \eta\rho_s\, dV, \quad M_f := \int_{\Omega_s} \rho_f\, dV = \int_{\Omega} \eta\rho_f\, dV, \tag{2.11}$$

and the indicator function η is defined as

$$\eta(t, \boldsymbol{x}) = \begin{cases} 1 & \boldsymbol{x} \in \overline{\Omega}_s(t), \\ 0 & \boldsymbol{x} \notin \overline{\Omega}_s(t). \end{cases} \tag{2.12}$$

To summarize, the two-way fluid-solid interaction problem of the freely falling solid body in an incompressible viscous fluid with a virtual force can be formulated as the following initial-boundary value problem: *find* $\boldsymbol{u}$, p, $\boldsymbol{F}$, $\boldsymbol{u}_c$ *and* ω *such that*

(2.13)
$$\begin{aligned}
\frac{\partial \boldsymbol{u}}{\partial t} - \nu\nabla^2\boldsymbol{u} + (\boldsymbol{u}\cdot\nabla)\boldsymbol{u} + \nabla p &= \boldsymbol{f} + \boldsymbol{F}, \quad t \in (0,T),\ \boldsymbol{x} \in \Omega, \\
\nabla\cdot\boldsymbol{u} &= 0, \quad t \in (0,T),\ \boldsymbol{x} \in \Omega, \\
\boldsymbol{u} &= \boldsymbol{u}_b, \quad t \in (0,T),\ \boldsymbol{x} \in \partial\Omega, \\
\boldsymbol{u} &= \boldsymbol{u}_0, \quad t = 0,\ \boldsymbol{x} \in \overline{\Omega}, \\
\boldsymbol{u} = \boldsymbol{u}_s &= \boldsymbol{u}_c + \omega \times \boldsymbol{r}, \quad t \in (0,T),\ \boldsymbol{x} \in \overline{\Omega}_s, \\
(M_s - M_f)\frac{d\boldsymbol{u}_c}{dt} + \int_{\Omega_s} \rho_f \boldsymbol{F}\, dV &= (M_s - M_f)\boldsymbol{g}, \quad \boldsymbol{u}_c(0) = \boldsymbol{u}_{c0}, \\
(I_s - I_f)\frac{d\omega}{dt} + \int_{\Omega_s} \rho_f \boldsymbol{r}\times\boldsymbol{F}\, dV &= 0, \quad \omega(0) = \omega_0,
\end{aligned}$$

where $\boldsymbol{u}_{c0}$ and ω_0 are the given initial values.

3. A simple collision model

It is unavoidable that the collisions may occur between solid objects or solid objects with the boundaries of container (walls) during the free-falling process. Therefore, the effect of collision should be taken into account in

the actual numerical simulations. In what follows, we will briefly introduce a simple collision model which was also considered in [4, 14] for describing the repulsion force arising from body-body or body-wall collisions in the fluid-solid interaction process.

We assume for simplicity that there are N_p solid objects (but not necessarily identical) immersed in fluid, all of which are two-dimensional circular particles and labelled as $1, 2, \cdots, N_p$. We assume that the repulsive force occurs whenever a particle is already touching or close enough to the other particles or the walls during the interaction process. The repulsive force will include a small parameter $\varepsilon_p > 0$ to control the size of the force and a small tolerance $\delta > 0$ to adjust the force effecting the system or not. We denote the total repulsive force by

$$\boldsymbol{F}^{co} := \boldsymbol{F}^{p} + \boldsymbol{F}^{w} := \sum_{i=1}^{N_p} \boldsymbol{F}_i^{p} + \sum_{i=1}^{N_w} \boldsymbol{F}_i^{w}, \tag{3.1}$$

where $\boldsymbol{F}^p$ is the repulsive force between particles and $\boldsymbol{F}^w$ is the repulsive force with the walls (labelled as $1, 2, \cdots, N_w$) that are respectively defined below. We define the repulsive force that particle i bears by

$$\boldsymbol{F}_i^{p} = \sum_{j=1, j\neq i}^{N_p} \boldsymbol{F}_{ij}^{p}, \tag{3.2}$$

where the repulsive force $\boldsymbol{F}_{ij}^p$, distributed only on the region of particle i, arising from the collision with particle j is given by

$$\boldsymbol{F}_{ij}^{p} = \begin{cases} \boldsymbol{0}, & d_{ij} > R_i + R_j + \delta, \\ \dfrac{\boldsymbol{X}_c^{(i)} - \boldsymbol{X}_c^{(j)}}{\varepsilon_p}(R_i + R_j + \delta - d_{ij})^2, & d_{ij} \leq R_i + R_j + \delta, \end{cases} \tag{3.3}$$

where $\boldsymbol{X}_c^{(i)}$ and R_i are respectively the coordinates of the center and the radius of particle i, while d_{ij} is the distance between the centers of particles i and j; see Figure 3.1 (left).

On the other hand, the repulsive force with walls that particle i bears is defined by

$$\boldsymbol{F}_i^{w} = \sum_{j=1}^{N_w} \boldsymbol{F}_{ij}^{w}, \tag{3.4}$$

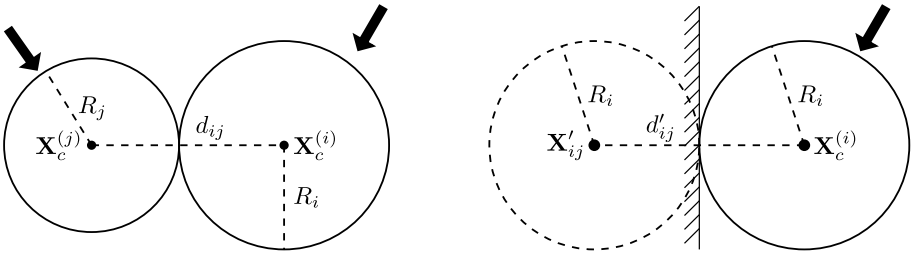

Figure 3.1: A schematic diagram of the collision model: (left) particle i collided with particle j; (right) particle i collided with wall j.

where N_w is the number of walls and $\boldsymbol{F}_{ij}^w$ is the repulsive force, distributed only on the region of particle i, coming from wall j is given by

$$\boldsymbol{F}_{ij}^w = \begin{cases} \mathbf{0}, & d'_{ij} > 2R_i + \delta, \\ \dfrac{\boldsymbol{X}_c^{(i)} - \boldsymbol{X}'_{ij}}{\varepsilon_w}(2R_i + \delta - d'_{ij})^2, & d'_{ij} \le 2R_i + \delta, \end{cases} \tag{3.5}$$

where $\varepsilon_w > 0$ is a small parameter to control the size of the force, $\boldsymbol{X}'_{ij}$ is the coordinates of the center of a fictitious particle with the same radius R_i inside and tangent to the wall j, and d'_{ij} is the distance between the centers of particle i and the fictitious particle; see Figure 3.1 (right).

Based on some physical models, Glowinski *et al.* [14] have indicated how to design the collision parameters ε_p, ε_w, and δ in the repulsive force. The explicit formulations of the parameters ε_p and ε_w can be found in [14] (see also [4]), and the range of the repulsive force δ is recommended to be taken of the order of the grid size parameter h of the numerical method.

Now, the induced total repulsive force $\boldsymbol{F}^{co}$ can be viewed as an additional momentum forcing term which should be integrated into the FSI problem (2.13). That is, the first equation in (2.13) should be replaced by

$$\frac{\partial \boldsymbol{u}}{\partial t} - \nu\nabla^2\boldsymbol{u} + (\boldsymbol{u}\cdot\nabla)\boldsymbol{u} + \nabla p = \boldsymbol{f} + \boldsymbol{F}^{co} + \boldsymbol{F}. \tag{3.6}$$

In addition, with this total repulsive force $\boldsymbol{F}^{co}$, similar to the derivation of the equations of motion (2.8)-(2.9), we find that the sixth equation in (2.13) should also be replaced by the following one:

$$(M_s - M_f)\frac{d\boldsymbol{u}_c}{dt} + \int_{\Omega_s} \rho_f \boldsymbol{F}\, dV = (M_s - M_f)(\boldsymbol{g} + \boldsymbol{F}^{co}), \quad \boldsymbol{u}_c(0) = \boldsymbol{u}_{c0}. \tag{3.7}$$

4. The direct-forcing immersed boundary projection method

In this section, we will present a new direct-forcing IB projection method which combines the direct-forcing approach with the Choi-Moin second-order in time projection scheme [5] for approximating the initial-boundary value problem (2.13). To simplify the presentation, in this section we temporarily ignore the repulsive force $\boldsymbol{F}^{co}$.

Let $t_i = i\Delta t$, $i = 0, 1, 2, \cdots$, with $\Delta t > 0$ be the time step length. We first consider the fluid part of (2.13), i.e., the system (2.1). The time integration of momentum equation for the fluid part (2.1) is performed by using a third-order low-storage Runge-Kutta formula for the convection term and a second-order Crank-Nicolson formula for the diffusion term [17, 16, 25]. More specifically, in the time interval $[t_n, t_{n+1}]$, a three-step time advancement scheme for the incompressible Navier-Stokes equations (2.1) in the absence of virtual force $\boldsymbol{F}$ can be posed as follows [25]: for $k = 1, 2, 3$, solve

$$
\begin{aligned}
&\frac{\boldsymbol{u}^k - \boldsymbol{u}^{k-1}}{\Delta t} - \alpha_k(\nu\nabla^2\boldsymbol{u}^k + \nu\nabla^2\boldsymbol{u}^{k-1}) + \\
&\quad \gamma_k[(\boldsymbol{u}\cdot\nabla)\boldsymbol{u}]^{k-1} + \xi_k[(\boldsymbol{u}\cdot\nabla)\boldsymbol{u}]^{k-2} + 2\alpha_k\nabla p^k &&= 2\alpha_k\boldsymbol{f}^{n+1} \quad \text{in } \Omega, \\
&\qquad\qquad \nabla\cdot\boldsymbol{u}^k &&= 0 \quad \text{in } \Omega, \\
&\qquad\qquad \boldsymbol{u}^k &&= \boldsymbol{u}_b \quad \text{on } \partial\Omega,
\end{aligned}
\tag{4.1}
$$

where the superscript k denotes the sub-step index, and $\boldsymbol{u}^0 := \boldsymbol{u}^n$ and $\boldsymbol{u}^{n+1} := \boldsymbol{u}^3$ are the velocity fields at time levels t^n and t^{n+1}, respectively. The coefficients α_k, γ_k and ξ_k for $k = 1, 2, 3$ are constants selected such the total time advancement between t_n and t_{n+1} is third-order accurate for convective term and second-order for the viscous term [17, 25]:

$$
\begin{aligned}
&\alpha_1 = 4/15, \quad \alpha_2 = 1/15, \quad \alpha_3 = 1/6; \\
&\gamma_1 = 8/15, \quad \gamma_2 = 5/12, \quad \gamma_3 = 3/4; \\
&\xi_1 = 0, \quad \xi_2 = -17/60, \quad \xi_3 = -5/12.
\end{aligned}
\tag{4.2}
$$

The advantages of this time-discretization scheme is that the numerical stability number $CFL = \Delta t\|\boldsymbol{u}\|_\infty/\Delta x$ is about $\sqrt{3}$ based on the total time step Δt (cf. [25]). That means it allows us to simulate the FSI problem using a larger time step length than our previous work [18] in which we used explicit Adams-Bashforth scheme to treat the nonlinear convection term.

We are now in a position to describe the direct-forcing IB projection method for the FSI problem (2.13).

A direct-forcing IB projection method: Suppose that at the beginning of time level $t = t_{n+1}$, the velocity field $\boldsymbol{u}^n$, the pressure p^n, the density of body force $\boldsymbol{f}^{n+1}$ and virtual force terms $\boldsymbol{F}^n$, $\boldsymbol{F}^{n-1}$, as well as the position $\boldsymbol{X}_c^n$, the translational velocity $\boldsymbol{u}_c^n$ and angular velocity ω^n of the falling solid object are all given. We then perform the following steps:

(S1) Compute the translational velocity $\boldsymbol{u}_c^{n+1}$ and angular velocity ω^{n+1} of the solid object by

$$\begin{aligned}
\frac{\boldsymbol{u}_c^{n+1} - \boldsymbol{u}_c^n}{\Delta t} &= \boldsymbol{g} - \frac{1}{M_s - M_f}\Big(\frac{3}{2}\int_{\Omega_s^n} \rho_f \boldsymbol{F}^n - \frac{1}{2}\int_{\Omega_s^{n-1}} \rho_f \boldsymbol{F}^{n-1}\Big), \\
\frac{\omega^{n+1} - \omega^n}{\Delta t} &= \frac{-1}{I_s - I_f}\Big(\frac{3}{2}\int_{\Omega_s^n} \rho_f \boldsymbol{r}^n \times \boldsymbol{F}^n - \frac{1}{2}\int_{\Omega_s^{n-1}} \rho_f \boldsymbol{r}^{n-1} \times \boldsymbol{F}^{n-1}\Big).
\end{aligned}$$

One can check that the above two schemes are second-order time-discretizationes of the two initial value problems in (2.13), respectively.

(S2) Compute the new position of the solid object by

$$\begin{aligned}
\boldsymbol{X}_c^{n+1} &= \boldsymbol{X}_c^n + \frac{\Delta t}{2}(\boldsymbol{u}_c^{n+1} + \boldsymbol{u}_c^n), \\
\theta^{n+1} &= \theta^n + \frac{\Delta t}{2}(\omega^{n+1} + \omega^n),
\end{aligned}$$

which are respectively the second-order in time implicit trapezoidal discretizations of the equations in (2.3).

(S3) Solve the system (4.1) for each sub-step $k = 1, 2, 3$ by using the Choi-Moin projection scheme as follows:

(3a) Solve for the intermediate velocity fields $\widetilde{\boldsymbol{u}}^k$ and $\boldsymbol{u}^*$ by

$$\begin{aligned}
&\frac{\widetilde{\boldsymbol{u}}^k - \boldsymbol{u}^{k-1}}{\Delta t} - \alpha_k(\nu\nabla^2\widetilde{\boldsymbol{u}}^k + \nu\nabla^2\boldsymbol{u}^{k-1}) + \\
&\gamma_k[(\boldsymbol{u}\cdot\nabla)\boldsymbol{u}]^{k-1} + \xi_k[(\boldsymbol{u}\cdot\nabla)\boldsymbol{u}]^{k-2} + 2\alpha_k\nabla p^{k-1} = 2\alpha_k\boldsymbol{f}^{n+1} \quad \text{in } \Omega, \\
&\widetilde{\boldsymbol{u}}^k = \boldsymbol{u}_b \quad \text{on } \partial\Omega, \\
&\frac{\boldsymbol{u}^* - \widetilde{\boldsymbol{u}}^k}{\Delta t} - 2\alpha_k\nabla p^{k-1} = \boldsymbol{0} \quad \text{in } \Omega.
\end{aligned}$$

(3b) Solve for the pressure increment φ^k by

$$\nabla^2\varphi^k = \frac{1}{2\alpha_k}\frac{1}{\Delta t}\nabla\cdot\boldsymbol{u}^* \quad \text{in } \Omega,$$

$$\nabla\varphi^k \cdot \boldsymbol{n} \quad = \quad 0 \quad \text{on } \partial\Omega,$$

and update the velocity field by

$$\boldsymbol{u}^k = \boldsymbol{u}^* - 2\alpha_k \Delta t \nabla\varphi^k.$$

(3c) Update the pressure by

$$p^k = \varphi^k - \frac{\nu}{2}\nabla \cdot \widetilde{\boldsymbol{u}}^k.$$

At the end of this step, we set $\boldsymbol{u}^{**} := \boldsymbol{u}^3$ and $p^{n+1} := p^3$.

(S4) In order to make the velocity of solid body region to cope with the solid velocity, we need an additional step to reset the velocity of solid body region to be the same as that of solid's velocity given by

$$\boldsymbol{u}_s^{n+1} = \boldsymbol{u}_c^{n+1} + \omega^{n+1} \times \boldsymbol{r}^{n+1} \quad \text{in } \overline{\Omega}_s^{n+1}.$$

This can be accomplished by first defining the virtual force in the whole solid body region as

$$\boldsymbol{F}^{n+1} := \eta \frac{\boldsymbol{u}_s^{n+1} - \boldsymbol{u}^{**}}{\Delta t} \quad \text{in } \Omega,$$

and then solve the velocity $\boldsymbol{u}^{n+1}$ by directly setting

$$\frac{\boldsymbol{u}^{n+1} - \boldsymbol{u}^{**}}{\Delta t} = \boldsymbol{F}^{n+1} \quad \text{in } \Omega,$$

where the indicator function $\eta(t_{n+1}, \boldsymbol{x})$ is given in (2.12). When the whole domain Ω is discretized using the Cartesian grids, η will denote the volume fraction of solid inside a cell and it is generally between 0 (pure fluid) and 1 (pure solid) and can be fractional for cells cut by immersed solid boundary [18].

5. Numerical experiments

In this section, we will perform several numerical experiments to illustrate the effectiveness of the direct-forcing IB projection method proposed in Section 4. In all these 2-D examples, we apply the second-order centered differences over a uniform staggered Cartesian grid for the space-discretizations in the projection scheme (cf. [10]). More specifically, the unknown functions

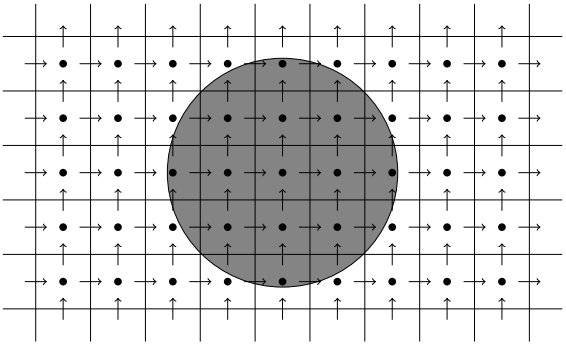

Figure 5.1: A schematic diagram of the computational domain Ω with a staggered Cartesian grid.

u and F_1, v and F_2, and p are approximated at the staggered grid points marked by $\rightarrow$, $\uparrow$ and $\bullet$, respectively; see Figure 5.1.

To validate the proposed method, we first consider the FSI problem of flow past a swimming fish-like solid body with a given varying solid shape and with a prescribed solid velocity. Then we examine examples of the falling of a single circular solid ball and two circular solid balls in a rectangular tank filled with an incompressible Newtonian viscous fluid. We also consider the sedimentation of a cloud of circular particles in a non-rectangular fluid domain to demonstrate the ability of the collision model for handling complicated collisions between particles and walls. In all examples, the density of body force of fluid is set to be zero, $\boldsymbol{f} = \mathbf{0}$.

5.1. Flow past a swimming fish-like solid body

In this example, we study the complex dynamics of a fish-like solid body, which takes a transverse prescribed motion, swimming in a uniform flow in a rectangular tank. We are given the varying shape of the solid body whose equilibrium position is represented by the contour of NACA0012 airfoil and the swimming motion of the solid body is governed by a backbone oscillation equation; see [9, 15] for more details. In Figure 5.2, we show the computational domain Ω with boundary conditions and the schematic diagram of the fish-like body.

The detailed settings of the simulation are given below:

- The Reynolds number is defined as $Re := U_\infty L/\nu$, where L is the chord length of the airfoil, U_∞ the free-stream velocity and ν the kinematic

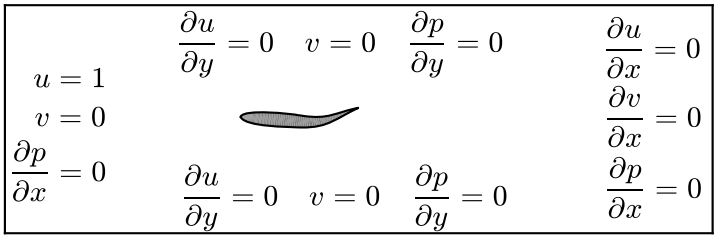

Figure 5.2: Boundary conditions of the FSI problem of flow past a swimming fish-like solid body.

viscosity. In this example, the characteristic velocity is $U_\infty = 1$, the chord line is $L = 1$, and the considered Reynolds number is $Re = 1/\nu = 5000$.

- The computational domain is taken as $\Omega = (-2L, 4L) \times (-L, L)$. The spatial mesh size is taken as $h = 1/480$, the time step $\Delta t = 2 \times 10^{-3}$, and the final time $T = 20$. Note that here our time step Δt is larger by 10 times than that used in [15].
- The midline of the fish-like solid body makes a lateral oscillation in the form

$$y_m(x,t) = A_m(x)\cos(2\pi(x-t)), \quad 0 \le x \le 1,$$

where A_m represents the amplitude and x is the position along the chord line. To model the backbone undulation during swimming, the amplitude A_m is approximated by a quadratic polynomial given by

$$A_m(x) = 0.02 - 0.0825x + 0.1625x^2.$$

The symmetrical shape of the fish-like body about the midline is described by the equation:

$$y(x) = 0.6\big(0.2969\sqrt{x} - 0.1260x - 0.3516x^2 + 0.2843x^3 - 0.1036x^4\big),$$

where $y(x)$ is the half thickness at a given value x, from the centerline to the solid body surface.

Numerical results of the instantaneous vorticity contours are shown in Figure 5.3, from which we can find that the proposed direct-forcing IB projection method is capable of simulating the complex dynamics of flow past a swimming fish-like solid body. In the vorticity contours, the flow wakes

Table 5.1: The comparison of convergent time step and CPU time of the RK3 and AB schemes employed in the proposed method for the time interval $[0, 4]$

time step Δt	2×10^{-3}	1×10^{-3}	8×10^{-4}	5×10^{-4}	CPU time
RK3 scheme	convergent	–	–	–	2627.39 s
AB scheme	divergent	divergent	divergent	convergent	4570.35 s

evolve behind the solid body as the time goes on. The wakes undulate up and down when the body oscillates. As the time goes further, the wakes get into a periodic behavior, which is very similar to that reported in [15].

As we have pointed out in Section 4 that for allowing a larger time step Δt in the time integration scheme, we employ a third-order low-storage Runge-Kutta scheme (RK3 scheme) [25] in the step (S3) of the proposed method, instead of using the usual explicit Adams-Bashforth scheme (AB scheme) [18] for the nonlinear convection term. A comparison of the convergent time step and the CPU time of these two different approaches is presented in Table 5.1, where we consider the RK3 scheme with $\Delta t = 2 \times 10^{-3}$ and the AB scheme with $\Delta t = 5 \times 10^{-4}$ for simulating the FSI problem of flow past a swimming fish-like solid body on the time interval $[0, 4]$. In the numerical computations, all the Helmholtz equations for intermediate velocity are solved by a preconditioned conjugate gradient scheme and all the Poisson equations for pressure increment are solved by the fast Fourier transform technique. Numerical results shows that the RK3 scheme is more efficient than the AB scheme. The CPU time of the RK3 scheme is much less than that of the AB scheme. This is because that the time step Δt of the RK3 scheme can be taken as about 4 times larger than that of the explicit AB scheme and the stability can be retained well, though the former needs to solve more Helmholtz equations and more Poisson equations than the latter. Another possible reason is that in the RK3 scheme, we employ the solution of the current sub-step as an initial guess for the preconditioned conjugate gradient iterations of the next sub-step, which is intuitively a good initial approximation in accelerating the convergence process.

To close this subsection, we plot in Figure 5.4 the instantaneous vorticity contours at time $t = 4$ produced by the proposed method with the RK3 and AB schemes. Clearly, both schemes show stable periodic behavior.

5.2. A single freely falling circular solid body

In this example, we consider a 2-D solid ball falling in a rectangular tank filled with an incompressible Newtonian viscous fluid. The settings of simula-

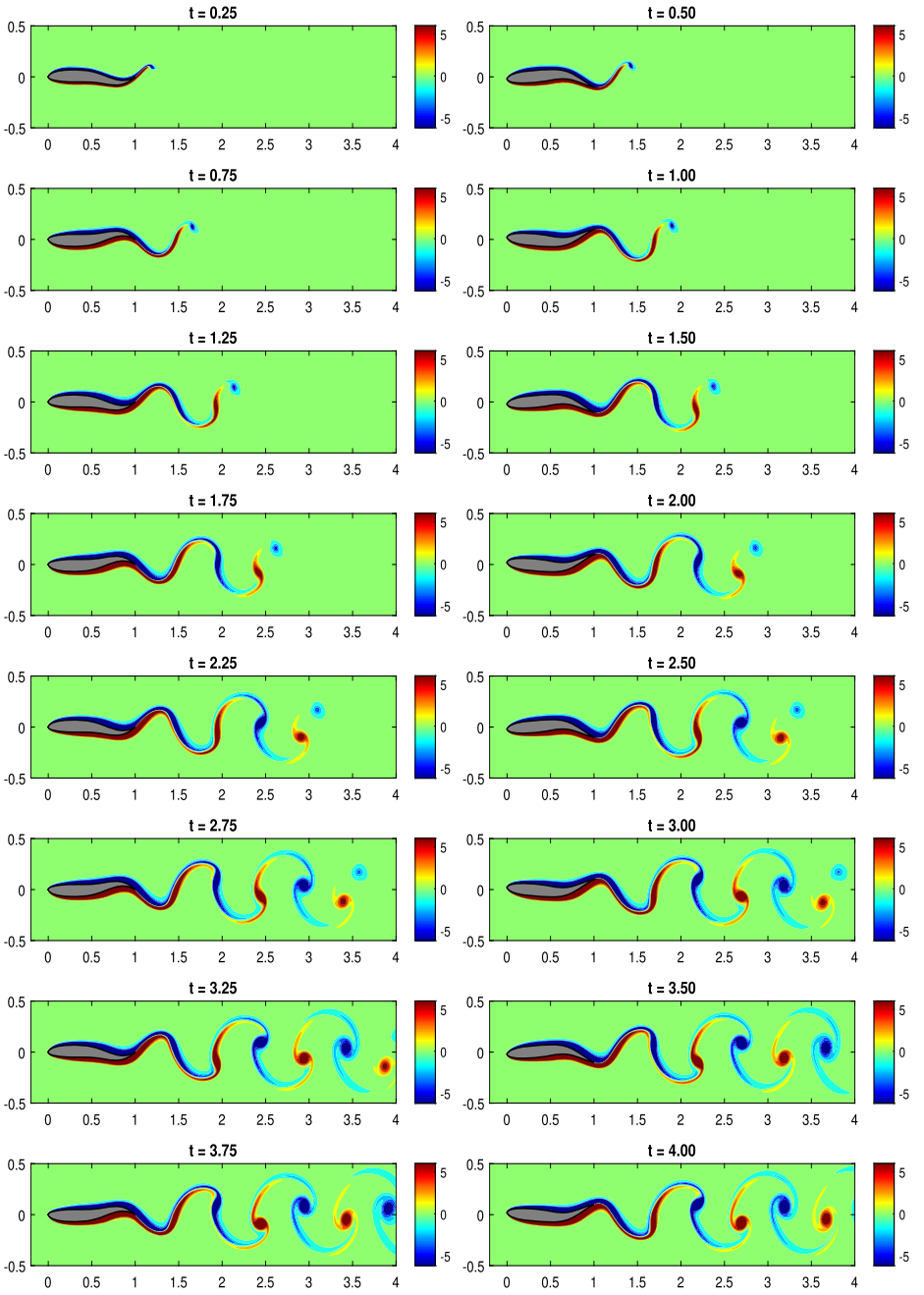

Figure 5.3: The instantaneous vorticity contours of the FSI problem of flow past a swimming fish-like solid body.

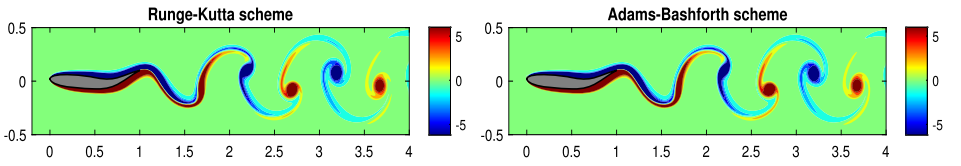

Figure 5.4: The instantaneous vorticity contours of the FSI problem of flow past a swimming fish-like solid body at time $t = 4$ produced by the proposed method with Runge-Kutta (left) and Adams-Bashforth (right) schemes.

tion are same with that in the work of Glowinski *et al.* [14]. More specifically, the settings of the simulation are given below:

- The computational domain is $\Omega := (0, 2) \times (0, 6)$, the diameter of the solid ball $\overline{\Omega}_s$ is $d = 0.25$ and the center is located at $(1, 4)$ at the initial time $t = 0$.
- We consider the initial condition $\boldsymbol{u}_0 = \mathbf{0}$ in Ω and the boundary function $\boldsymbol{u}_b = \mathbf{0}$ on $\partial\Omega$ for all time.
- The density of fluid part is $\rho_f = 1$ and solid part is $\rho_s = 1.5$, the fluid viscosity is $\nu = 0.01$, and the gravity is taken as $\boldsymbol{g} = (0, -980)$.
- We take the grid size $h = 1/256$ and the time step $\Delta t = 10^{-4}$.
- The collision parameter ε_w in the repulsive force (3.4) with the bottom of tank is taken as $\varepsilon_w = 10^{-7}$ and the tolerance distance is taken as $\delta = 2h$.

In the above settings, the tolerance distance is taken as $\delta = 2h$ which is recommended by Blasco *et al.* [4]; see also [14]. However, the choice of the collision parameter $\varepsilon_w = 10^{-7}$ (and another collision parameter $\varepsilon_p = 10^{-7}$ in the next two subsections) is based on our numerical experience, which is larger than that suggested in [14] and consequently, the repulsive force is relatively small in the present paper. In addition, we note that the stability of the proposed method seems not to be affected by these small parameters as long as the repulsive force is not too large.

Numerical results of the position of freely falling solid ball and the flow field visualization at different times are displayed in Figure 5.5. Furthermore, the time evolution of position and translational velocity of the solid ball in y-component compared with the results of Glowinski *et al.* [14] and Horng *et al.* [18] are depicted in Figure 5.6, from which we can find that the results produced by the proposed method are in very well agreement with that in [14] with the finer grid size $h = 1/384$, and obviously better than that presented in [18].

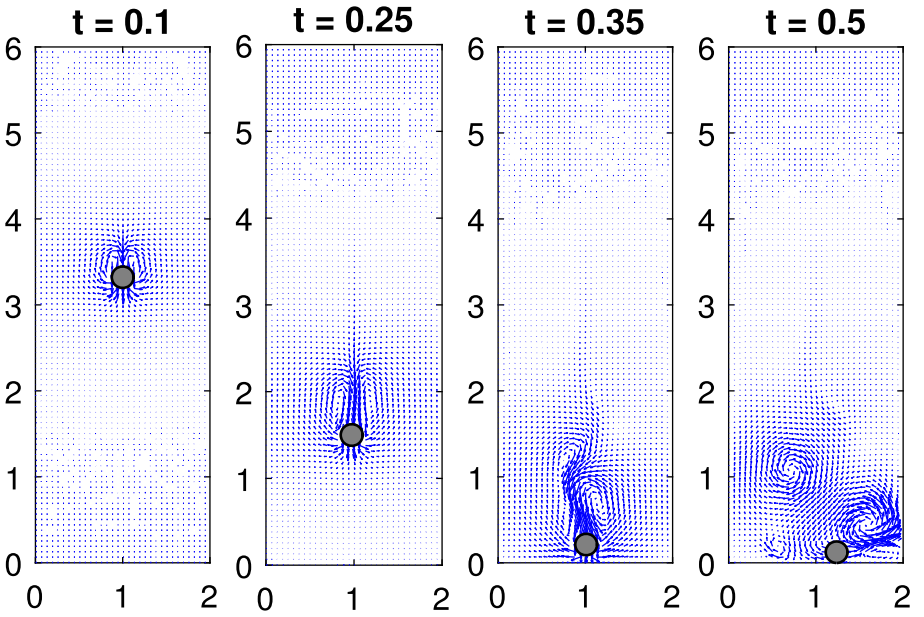

Figure 5.5: The position of freely falling solid ball and the flow field visualization at time $t = 0.1, 0.25, 0.35, 0.5$.

5.3. Two freely falling circular solid bodies

In this example, we simulate two identical balls freely falling in the fluid to study the drafting, kissing and tumbling phenomena [4, 14, 26, 42]. To demonstrate these interesting phenomena, we consider the following settings:

- The computational domain, initial and boundary conditions are taken the same as the case of single free-falling ball in Subsection 5.2.
- The fluid density is $\rho_f = 1$, the fluid viscosity is $\nu = 0.01$, and the gravity is taken as $\boldsymbol{g} = (0, -980)$.
- These two identical solid balls are respectively centered at $(1 - 0.001, 4.5)$ and $(1 + 0.001, 5)$ at time $t = 0$ and both with diameter $d = 0.25$ and density $\rho_s = 1.5$.
- The time step size is $\Delta t = 10^{-4}$ and the spatial mesh size is $h = 1/256$.
- The collision parameters in the total repulsive force (3.1) are given by $\varepsilon_w = 10^{-7}$, $\varepsilon_p = 10^{-7}$, and the tolerance distance $\delta = 2h$.

From the numerical results presented in Figure 5.7, we observe that the falling process is qualitatively consistent with the experimental results reported in [13]. At first, each ball has the same acceleration by gravitational

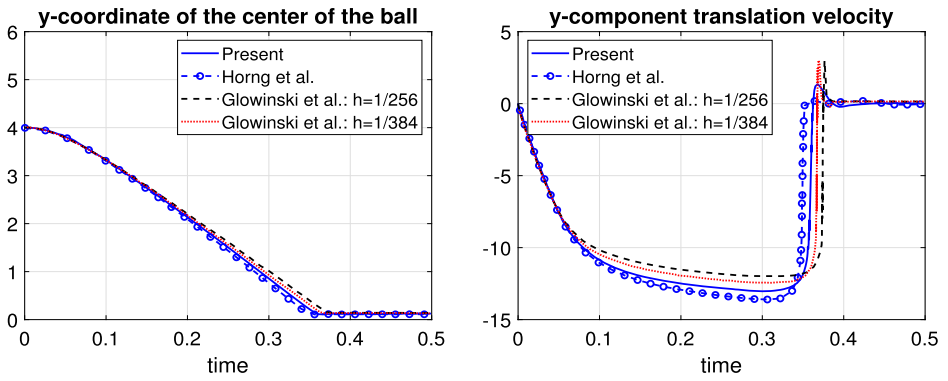

Figure 5.6: The time evolution of position (left) and translational velocity (right) of the freely falling solid ball in y-component compared with the results of Glowinski *et al.* [14] and Horng *et al.* [18].

force. Then the velocity of the upper ball becomes faster than that of the lower ball because of the lower ball undergoes more resistant against the fluid comparing to the upper one as time goes on. Consequently, the lower ball drafts the upper ball and then the two balls become kissing to be combined together like an elongated rigid body. However, at this moment, some instability arises in the motion of the combined ball, so that it has a tendency to rotate. Finally, the upper ball tumbles over the lower ball and two balls are separated apart from each other.

More specifically, as shown in the Figure 5.7, the upper ball becomes falling faster than that of the lower ball at $t = 0.1$ (drafting). About $t = 0.18$, the upper ball touches the lower one (kissing). But the combined ball is unstable and the two balls separate at about $t = 0.22$. After all, the upper ball tumbles over the lower ball at $t = 0.26$ (tumbling). These numerical results are similar to those obtained in the literature [4, 14, 26, 42]. For experimental results, we refer the reader to [13].

5.4. Sedimentation of multiple particles

In this example, we consider the sedimentation of a cloud of small circular particles in a non-rectangular fluid domain. This example will demonstrate the good ability of the simple collision model described in Section 3 for simulating complicated collisions between the falling particles and particles with walls. The settings of the simulation are given as follows:

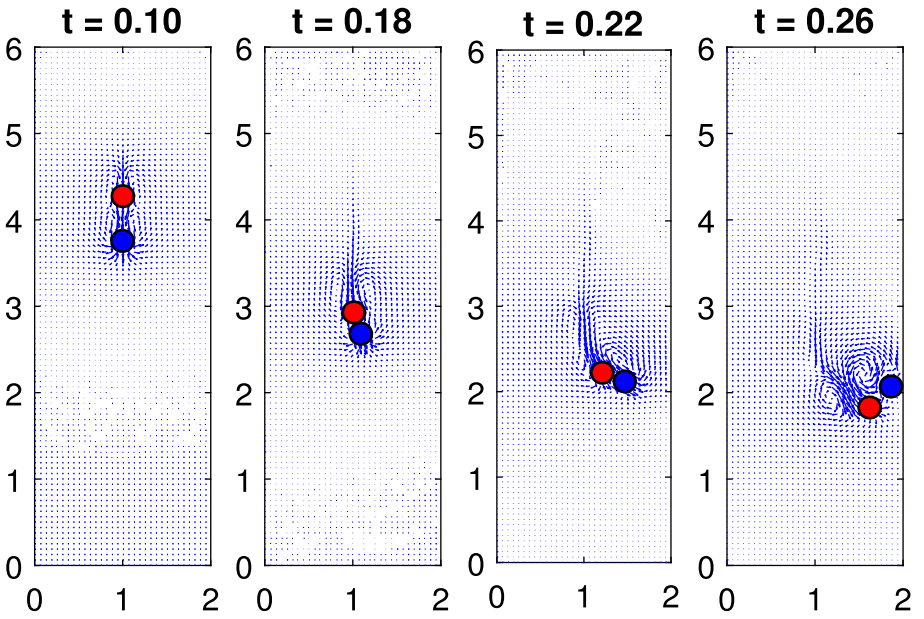

Figure 5.7: The positions of two freely falling solid balls and the flow field visualization at time $t = 0.1$ (drafting), $t = 0.18$ (kissing), $t = 0.22$, and 0.26 (tumbling).

- The computational domain is same as that used in Subsection 5.2 and Subsection 5.3, except that there is a slope at the bottom, that is, $\Omega := (0, 2) \times (0, 6) \setminus \{(x, y) : x, y \geq 0, x + y \leq 1\}$.
- There are 10 rows of identical particles at the top of cavity, and each row has 10 particles of diameter $d = 0.15$ at the initial time $t = 0$. We consider the initial condition $\boldsymbol{u}_0 = \mathbf{0}$ in Ω and the boundary function $\boldsymbol{u}_b = \mathbf{0}$ on $\partial\Omega$ for all time.
- The fluid density is $\rho_f = 1$ and the particles density are all $\rho_s = 1.5$. The fluid viscosity is $\nu = 0.01$ and the gravity is $\boldsymbol{g} = (0, -980)$.
- The time step size is $\Delta t = 10^{-4}$ and the spatial mesh size is $h = 1/256$. The collision parameters in the total repulsive force (3.1) are given by $\varepsilon_w = 10^{-7}$, $\varepsilon_p = 10^{-7}$, and the tolerance distance $\delta = 2h$.

The numerical results are displayed in Figure 5.8. We can find that the proposed direct-forcing IB projection method can handle the complicated collisions of the multiple falling particles system very well, and the sedimentation process can be successfully simulated.

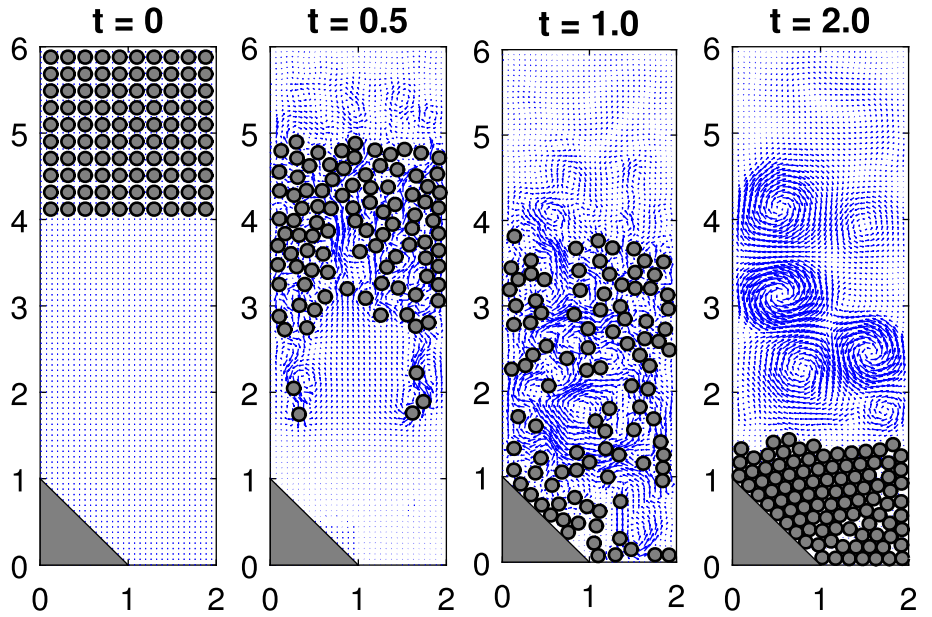

Figure 5.8: The sedimentation of multiple particles and the flow field visualization at time $t = 0, 0.5, 1.0,$ and 2.0.

6. Summary and conclusion

In this paper, we have successfully developed a new direct-forcing IB approach combined with the second-order in time Choi-Moin projection scheme to simulate the dynamical behavior of freely falling solid bodies in an incompressible viscous fluid. The basic idea of the direct-forcing approach is that we first regard the solid object region as made of fluid and then introduce a momentum forcing distributed only on that region that enforces the region to behave like a real solid body with the solid velocity.

In the proposed method, we have used a third-order Runge-Kutta formula for the convection and a second-order Crank-Nicolson formula for the diffusion to discretize the time variable in the momentum equation. Moreover, we have employed second-order centered differences over a staggered Cartesian grid for all the spatial discretizations in the projection scheme. We have also integrated a collision model into the method for circular particles to mimic the repulsion force arising from body-body or body-wall collisions. The most advantageous feature of this method is that it is conceptually simple and rather easy to implement, without involving any discrete Dirac

delta functions or any post interpolations for accuracy like most IB methods in the literature. We have presented several numerical examples to illustrate the effectiveness of the newly proposed method. From the numerical results, we have found that this direct-forcing IB projection method is capable of simulating the complex behavior of two-way FSI problems.

To conclude this paper, we remark that the proposed direct-forcing IB projection approach can also be applied to study the heat transfer process in thermal FSI problems, provided we additionally introduce an appropriate virtual heat source to the energy transport equation. This issue deserves further investigation.

Acknowledgments

The authors would like to thank the anonymous referees for their valuable comments and suggestions that led to a substantial improvement of the original manuscript.

References

[1] A. Andersen, U. Pesavento, and Z. J. Wang, Unsteady aerodynamics of fluttering and tumbling plates, *Journal of Fluid Mechanics,* 541 (2005), pp. 65–90. MR2262644

[2] A. Andersen, U. Pesavento, and Z. J. Wang, Analysis of transitions between fluttering, tumbling and steady descent of falling cards, *Journal of Fluid Mechanics,* 541 (2005), pp. 91–104. MR2262645

[3] A. Belmonte, H. Eisenberg, and E. Moses, From flutter to tumble: inertial drag and Froude similarity in falling paper, *Physical Review Letters,* 81 (1998), pp. 345–348.

[4] J. Blasco, M. C. Calzada, and M. Marín, A fictitious domain, parallel numerical method for rigid particulate flows, *Journal of Computational Physics,* 228 (2009), pp. 7596–7613. MR2561833

[5] H. Choi and P. Moin, Effects of the computational time step on numerical solutions of turbulent flow, *Journal of Computational Physics,* 113 (1994), pp. 1–4.

[6] A. J. Chorin, Numerical solution of the Navier-Stokes equations, *Mathematics of Computation,* 22 (1968), pp. 745–762. MR0242392

[7] A. J. Chorin, On the convergence of discrete approximations to Navier-Stokes equations, *Mathematics of Computation,* 23 (1969), pp. 341–353. MR0242393

[8] F. Domenichini, On the consistency of the direct forcing method in the fractional step solution of the Navier-Stokes equations, *Journal of Computational Physics,* 227 (2008), pp. 6372–6384. MR2418365

[9] G.-J. Dong and X.-Y. Lu, Characteristics of flow over traveling wavy foils in a side-by-side arrangement, *Physics of Fluids,* 19 (2007), 057107.

[10] W. E and J.-G. Liu, Projection method III: spatial discretization on the staggered grid, *Mathematics of Computation*, 71 (2001), pp. 27–47. MR1862987

[11] E. A. Fadlun, R. Verzicco, P. Orlandi, and J. Mohd-Yusof, Combined immersed-boundary finite-difference methods for three-dimensional complex flow simulations, *Journal of Computational Physics,* 161 (2000), pp. 35–60. MR1762073

[12] D. L. Finn, Falling paper and flying business cards, *SIAM News,* 40 (2007), pp. 1–3.

[13] A. F. Fortes, D. D. Joseph, and T. S. Lundgren, Nonlinear mechanics of fluidization of beds of spherical particles, *Journal of Fluid Mechanics,* 177 (1987), pp. 467–483.

[14] R. Glowinski, T. W. Pan, T. I. Hesla, D. D. Joseph, and J. Periaux, A fictitious domain approach to the direct numerical simulation of incompressible viscous flow past moving rigid bodies: application to particulate flow, *Journal of Computational Physics,* 169 (2001), pp. 363–426. MR1836521

[15] A. Gronskis and G. Artana, A simple and efficient direct forcing immersed boundary method combined with a high order compact scheme for simulating flows with moving rigid boundaries, *Computers & Fluids,* 124 (2016) pp. 86–104. MR3430089

[16] S. Ha, J. Park, and D. You, A GPU-accelerated semi-implicit fractional-step method for numerical solutions of incompressible Navier-Stokes equation, *Journal of Computational Physics*, 352 (2018), pp. 246–264. MR3717136

[17] S. Hahn, J. Je, and H. Choi, Direct numerical simulation of turbulent channel flow with permeable walls, *Journal of Fluid Mechanics*, 450 (2002), pp. 259–285.

[18] T.-L. Horng, P.-W. Hsieh, S.-Y. Yang, and C.-S. You, A simple direct-forcing immersed boundary projection method with prediction-correction for fluid-solid interaction problems, *Computers & Fluids,* 176 (2018), pp. 135–152. MR3886364

[19] C. Jin and K. Xu, Numerical study of the unsteady aerodynamics of freely falling plates, *Communications in Computational Physics,* 3 (2008), pp. 834–851. MR2433336

[20] M. A. Jones and M. J. Shelley, Falling cards, *Journal of Fluid Mechanics,* 540 (2005), pp. 393–425. MR2263133

[21] T. Kajishima, S. Takiguchi, H. Hamasaki, and Y. Miyake, Turbulence structure of particle-laden flow in a vertical plane channel due to vortex shedding, *JSME International Journal, Series B,* 44 (2001), pp. 526–535.

[22] T. Kajishima and S. Takiguchi, Interaction between particle clusters and particle-induced turbulence, *International Journal of Heat and Fluid Flow,* 23 (2002), pp. 639–646.

[23] J. Kim, D. Kim, and H. Choi, An immersed-boundary finite-volume method for simulations of flow in complex geometries, *Journal of Computational Physics,* 171 (2001), pp. 132–150. MR1843643

[24] J. Kim and P. Moin, Application of a fractional-step method to incompressible Navier-Stokes equations, *Journal of Computational Physics,* 59 (1985), pp. 308–323. MR0796611

[25] H. Le and P. Moin, An improvement of fractional step methods for the incompressible Navier-Stokes equations, *Journal of Computational Physics,* 92 (1991), pp. 369–379.

[26] T.-R. Lee, Y.-S. Chang, J.-B. Choi, D. W. Kim, W. K. Liu, and Y.-J. Kim, Immersed finite element method for rigid body motions in the incompressible Navier-Stokes flow, *Computer Methods in Applied Mechanics and Engineering,* 197 (2008), pp. 2305–2316. MR2412827

[27] C.-C. Liao, Y.-W. Chang, C.-A. Lin, and J. M. McDonough, Simulating flows with moving rigid boundary using immersed-boundary method, *Computers & Fluids,* 39 (2010), pp. 152–167.

[28] C.-C. Liao, W.-W. Hsiao, T.-Y. Lin, and C.-A. Lin, Simulations of two sedimenting-interacting spheres with different sizes and initial configurations using immersed boundary method, *Computational Mechanics,* 55 (2015), pp. 1191–1200. MR3356140

[29] L. Mahadevan, W. S. Ryu, and A. D. T. Samuel, Tumbling cards, *Physics of Fluids,* 11 (1999), pp. 1–3.

[30] J. C. Maxwell, *The Scientific Papers of James Clerk Maxwell,* Dover, New York, 1890, pp. 115–118.

[31] R. Mittal and G. Iaccarino, Immersed boundary methods, *Annual Review of Fluid Mechanics,* 37 (2005), pp. 239–261. MR2115343

[32] R. Mittal, V. Seshadri, and H. S. Udaykumar, Flutter, tumble and vortex induced autorotation, *Theoretical and Computational Fluid Dynamics,* 17 (2004), pp. 165–170.

[33] J. Mohd-Yusof, *Interaction of Massive Particles with Turbulence,* Ph.D. Dissertation, Department of Mechanical and Aerospace Engineering, Cornell University, 1996.

[34] D. Z. Noor, M.-J. Chern, and T.-L. Horng, An immersed boundary method to solve fluid-solid interaction problems, *Computational Mechanics,* 44 (2009), pp. 447–453.

[35] D. Z. Noor, M.-J. Chern, and T.-L. Horng, Study of a freely falling ellipse with a variety of aspect ratios and initial angles, *Proceedings of the 22nd International Conference on Parallel Computational Fluid Dynamics,* Kaohsiung, Taiwan, May 17–21, 2010.

[36] T.-W. Pan, D. D. Joseph, and R. Glowinski, Simulating the dynamics of fluid-ellipsoid interactions, *Computers & Structures,* 83 (2005), pp. 463–478.

[37] U. Pesavento and Z. J. Wang, Falling paper: Navier-Stokes solutions, model of fluid forces, and center of mass elevation, *Physical Review Letters,* 93 (2004), 144501.

[38] C. S. Peskin, Flow patterns around heart valves: a numerical method, *Journal of Computational Physics,* 10 (1972), pp. 252–271. MR0475298

[39] C. S. Peskin, The immersed boundary method, *Acta Numerica,* 11 (2002), pp. 479–517. MR2009378

[40] P. Singh, D. D. Joseph, T.I. Hesla, R. Glowinski, T.-W. Pan, A distributed Lagrange multiplier/fictitious domain method for viscoelastic particulate flows, *Journal of Non-Newtonian Fluid Mechanics,* 91 (2000), pp. 165–188. MR2436653

[41] S.-W. Su, M.-C. Lai, and C.-A. Lin, An immersed boundary technique

for simulating complex flows with rigid boundary, *Computers & Fluids,* 36 (2007), pp. 313–324.

[42] M. Uhlmann, An immersed boundary method with direct forcing for the simulation of particulate flows, *Journal of Computational Physics,* 209 (2005), pp. 448–476. MR2151992

[43] J. Yang and F. Stern, A simple and efficient direct forcing immersed boundary framework for fluid-structure interactions, *Journal of Computational Physics,* 231 (2012), pp. 5029–5061. MR2929932

[44] J. Yang and F. Stern, A non-iterative direct forcing immersed boundary method for strongly-coupled fluid-solid interactions, *Journal of Computational Physics,* 295 (2015), pp. 779–804. MR3345235

[45] Z. Yu and X. Shao, A direct-forcing fictitious domain method for particulate flows, *Journal of Computational Physics,* 227 (2007), pp. 292–314.

Po-Wen Hsieh
Department of Applied Mathematics
National Chung Hsing University
South District, Taichung City 40227
Taiwan
E-mail address: pwhsieh@nchu.edu.tw

Suh-Yuh Yang
Department of Mathematics
National Central University
Jhongli District, Taoyuan City 32001
Taiwan
E-mail address: syyang@math.ncu.edu.tw

Cheng-Shu You
Department of Applied Mathematics
Feng Chia University
Xitun District, Taichung City 40724
Taiwan
E-mail address: csyou@fcu.edu.tw

Received August 12, 2019